

mmComb: High-speed mmWave Commodity WiFi Backscatter

Yoon Chae and Zhenzhe Lin, George Mason University; Kang Min Bae and Song Min Kim, Korea Advanced Institute of Science and Technology (KAIST);

Parth Pathak, George Mason University

https://www.usenix.org/conference/nsdi24/presentation/chae

This paper is included in the Proceedings of the 21st USENIX Symposium on Networked Systems Design and Implementation.

April 16–18, 2024 • Santa Clara, CA, USA

978-1-939133-39-7

Open access to the Proceedings of the 21st USENIX Symposium on Networked Systems Design and Implementation is sponsored by



mmComb: High-speed mmWave Commodity WiFi Backscatter

Yoon Chae[†], Zhenzhe Lin[†], Kang Min Bae[§], Song Min Kim[§], and Parth Pathak[†] *George Mason University*, [§] *Korea Advanced Institute of Science and Technology*

Abstract

High-speed connectivity is key to enabling a range of novel IoT applications. Millimeter-wave (mmWave) backscatter has emerged as a possible solution to create high-speed, low-power IoT networks. However, state-of-the-art mmWave backscatter systems are costly due to the need for dedicated mmWave reader devices. This paper presents mmComb, a mmWave backscatter system that is built to operate on commodity mmWave WiFi. mmComb is developed with the aim that mmWave backscatter tags can be directly integrated into 802.11ad/ay mmWave WiFi networks. mmComb makes two key contributions. First, We propose a technique to communicate with backscatter tags using existing beamforming protocol frames from mmWave WiFi devices, without any protocol modification. Second, we develop a self-interference suppression solution that intelligently uses receive beamforming to extract weak mmWave backscatter signal even in indoor multipath-rich channels. We implement our solution with a tag prototype and 60 GHz commodity WiFi devices. Our results show that mmComb can achieve a maximum data rate of 55 Mbps just by leveraging 802.11ad/ay control frames while consuming 87.3 μ W with BER lower than 10^{-3} up to 5.5 m range.

1 Introduction

The number of Internet-of-Things (IoT) devices is anticipated to grow close to 30 billion by 2030 [1], creating a wide range of novel applications enabled through high-speed edge and cloud connectivity. Examples of such applications include immersive computing and mixed reality, AI-assisted cyberphysical systems like autonomous vehicles, smart homes, and many more. Millimeter-wave (mmWave) wireless is at the forefront of designing 6G and beyond networks that can enable high-speed connectivity to IoT devices. However, today's mmWave devices consume a significant amount of energy (several watts in 802.11ad and 5G NR devices [39]). Hence, the majority of IoT devices (e.g., RFID, WiFi backscatter) operate in the sub-6 GHz spectrum. While the power consumption of such devices can be in tens of microwatts, their data rates are limited to a few kilobits per second [3, 17, 25] or even bits per second [8, 46, 56] in some cases. mmWave backscatter has emerged as a potential solution to bridge this gap and to enable high-speed, ultra-low-power IoT connectivity using the large bandwidths available in mmWave bands. A key limitation of prior work on mmWave backscatter [6, 23, 28, 41] is that they are not compliant with existing mmWave networks. This means that their adaptation requires either deploying dedicated readers in the network or non-trivial hardware and protocol modifications, increasing the overall cost and reducing their adaptability. For example, Millimetro [41] and OmniScatter [6] use mmWave FMCW radars as mmWave backscatter readers. While the objectives of these works are high-precision localization and massivescale IoT deployment, deployment of dedicated radars not only increases the cost but also creates non-trivial interference to existing mmWave networks [50]. mmTag [28], on the other hand, aims at high-speed mmWave backscatter but cannot achieve truly commodity operations. mmTag requires additional dedicated hardware (polarized antenna) on the transceiver to receive the polarized backscatter signal. It also requires a custom antenna with separate polarization on the AP and tags for self-interference suppression. Furthermore, the impact of integrating mmTag in mmWave networks is not clear given that it is not designed to be protocol compliant where specific frames are used for piggybacking the backscatter data. These limitations call for a new mmWave backscatter solution that is high-speed, ultra-low-power, and truly compatible with mmWave commodity networks by design.

In this paper, we present mmComb, a high-speed mmWave commodity WiFi backscatter system. mmComb is developed with the aim that mmWave backscatter tags can be seamlessly integrated into 802.11ad/ay mmWave WiFi networks. mmComb tags embed backscatter data bits by exploiting beamforming training frames that are frequently exchanged between 802.11ad/ay APs and clients. mmComb does not require any changes to mmWave WiFi APs or clients in terms of their hardware (no additional RF chains or custom antenna) or protocol stack, making it possible to directly accommodate mmWave backscatter tags into existing mmWave WiFi networks. mmComb can achieve a maximum data rate of 55 Mbps when leveraging 802.11ad beamforming frames for backscattering which is orders of magnitude higher than state-of-the-art sub-6 GHz WiFi backscatter systems [3, 17, 25, 53-55]. Our observed BER is lower than 10^{-3} for a range up to 5.5 m, enabling many practical applications within WLANs. Furthermore, the tag consumes 87.3 μW (10.5 μW only for modulation) including frame detection and modulation. We demonstrate an end-to-end backscatter system using a tag prototype and commercial offthe-shelf 802.11ad AP and clients acting as readers. mmComb addresses the following important challenges:

	Systems	Frequency band	Commodity WiFi compatible?	Data rate	Power consumption (μW)	
sub-6 GHz	WiFi backscatter [17]	2.4 GHz	Yes	1 Kbps	24	
	WiTAG [3]	2.4, 5 GHz	Yes	4 Kbps	10	
	MOXcatter [55]	2.4 GHz	Yes 50 Kbps		33	
	Freerider [54]	2.4 GHz	Yes	60 Kbps	30	
	Hitchhike [53]	2.4 GHz	Yes	300 Kbps	33	
mmWave	MilliMetro [41]	24 GHz	No (FMCW)	300 bps	2.36	
	OmniScatter [6]	24, 60 GHz	No (FMCW)	150 Kbps	7	
	mmX [27]	24 GHz	No (Dedicated reader)	100 Mbps	1.1×10^4	
	mmTag [28]	24 GHz	No (Dedicated reader)	100 Mbps	0.2×10^4	
	mmComb	60 GHz	Yes	55 Mbps	87.3	

Table 1: Comparison with state-of-the-art systems.

There are three key questions here: (i) which mmWave WiFi frames to use for backscatter communication?, (ii) how to detect the ongoing transmission of these frames?, and (iii) how to modulate and demodulate the backscatter data onto the frame? To answer the first question, mmComb selects 802.11ad/ay control frames, specifically beamforming frames, for backscatter communication. These frames are regularly transmitted (beacons, sector-level sweep, beam refinement, etc.) for beamforming and their reuse for backscattering creates no additional network overhead. Furthermore, they have relatively static structures and are transmitted in all directions (i.e., sectors) which improves demodulation and tag coverage. mmComb introduces an ultra-light detection technique for beamforming frames in tags by intelligently utilizing the unique differences between data and beamforming frames.

The tags then perform symbol inversion on incoming symbols

using phase shifting to modulate the backscatter data. The

backscatter bits are then extracted by determining the change

in the channel (estimated vs. measured) at the receiver.

(1) Embedding backscatter bits in mmWave WiFi frames.

(2) Suppressing self-interference. Another key challenge in mmWave backscatter is that due to high attenuation at mmWave frequencies, the backscattered mmWave signal is weak, making it very difficult to isolate the backscatter symbols from self-interference (i.e., the signal traveling directly from a transmitter to a receiver over LoS or reflected paths). Prior WiFi backscatter systems operating at sub-6 GHz such as HitchHike [53-55] address this issue by shifting the frequency of the backscattered signal to the adjacent WiFi channel. However, mmWave WiFi channels are 2.16 GHz wide, and switching such a channel would require a high-speed oscillator consuming as much as 0.5 mW which is clearly infeasible for a low-power tag [21]. Changing the polarization of the incoming and outgoing signal is another approach presented in [28]. However, such a solution requires non-trivial modifications to WiFi APs to equip them with differently polarized antennas and multiple switches on the tag (increased power consumption). Such solutions cannot be readily adapted to work with commodity mmWave WiFi networks.

mmComb addresses this challenge by exploiting the directionality of mmWave beams to create high-gain receive beams

at the receiver towards the desired tag while creating nulls in the direction of self-interference. Using the unique characteristics of beamforming antennas, mmComb eliminates the self-interference without shifting the center frequency. A salient benefit of this approach is that it requires no specialized hardware or protocol modifications in mmWave WiFi devices. Table 1 compares mmComb with state-of-the-art sub-6 GHz WiFi and mmWave backscatter systems.

(3) Tag prototyping, implementation and evaluation. We develop a custom prototype of mmComb tag with high switching speed (up to 100 MHz), capable of modulating the 802.11ad/ay frames at 55 MHz speed. We use off-the-shelf 802.11ad devices and software radios equipped with phased arrays as readers. We evaluate mmComb in diverse scenarios with extensive experiments. Our experiments show that mm-Comb can achieve a data rate of 55 Mbps using 802.11ad control frames with BER lower than 10^{-3} up to the 5.5m range. We also demonstrate that the control frames with backscatter data embedded in them can be received on an unmodified 802.11ad receiver. We find that our self-interference suppression technique, which beamforms towards a tag while creating nulls towards self-interference directions, provides over 19 dB increase in backscatter SINR compared to beams used in commodity 802.11ad/ay devices. mmComb's self-interference suppression is extensively evaluated (i.e., the impact of phase resolution, spatial smoothing, multiple self-interference paths, and different types of receiver devices). Our results show that even in environments with severe multi-path (3-5 reflected mmWave paths), the average BER remains low (6.5×10^{-3}) due to our self-interference suppression solution. We demonstrate that practical deployments of mmComb are feasible as they can support not only Line-of-Sight (LoS) but also Non-Line-of-Sight (NLoS) paths (tag behind a cardboard box or in an office cubicle). mmComb can scale to multiple tags densely deployed in the environment with very low inter-tag interference. Lastly, we verify that backscattering from the tag does not negatively impact standards-compliant beamforming.

Contributions. Our main technical contributions are:

mmComb is the first mmWave commodity WiFi backscatter system where the tags can seamlessly integrate into mmWave WiFi networks without any hardware or protocol

modifications.

- We present a self-interference suppression technique that can use beamforming and nulling to significantly improve SINR otherwise weak mmWave backscatter signal reception.
- mmComb is implemented with a custom tag prototype and commodity off-the-shelf 802.11ad devices as readers. We extensively evaluate mmComb in a diverse set of scenarios demonstrating the feasibility of high-speed, low-power mmWave commodity WiFi backscatter.

2 Background

A typical backscatter system consists of a reader and a tag where the reader sends an excitation query signal which is then reflected back by a tag. A tag can switch between different impedances to modulate the amplitude, phase, or frequency [9, 11] of the backscattered signal. In the case of commodity WiFi backscatter, an existing commodity device (e.g., a WiFi AP or client [53, 54]) in the wireless network operates as the reader, thus eliminating the need to deploy dedicated readers and reducing cost. Existing protocol frames transmitted from the commodity readers can also be retrofitted to create the query signal. In mmComb, mmWave WiFi 802.11 ad/ay devices and protocol frames are used for enabling high-speed mmWave backscatter communication. To this end, we now provide a brief background on mmWave WiFi.

802.11ad/ay DMG beamforming. The 60 GHz Directional Multi-Gigabit (DMG) mmWave 802.11ad/ay WiFi provides multi-gigabit-per-second data rate. Due to the high attenuation experienced at mmWave frequencies, directional beams created through phased antenna arrays are commonly utilized. Fig. 1 shows the beamforming training process [32, 35] that is used to determine the best transmit sector (i.e., beam pattern) pair between an AP and a station (STA). The procedure

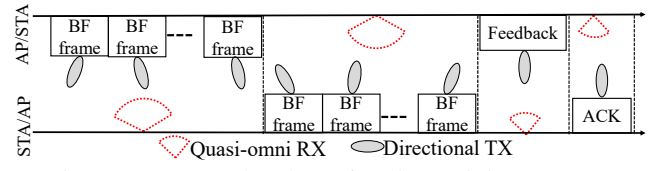


Figure 1: 802.11ad/ay beamforming training process.

involves sending beamforming (BF) frames from the AP in different sectors, and the station measures the received SNR for each. Then, the station sends the BF frames back to the AP, which measures the SNR. The feedback conveys the Tx sector with the highest SNR measurement from both AP to station and vice versa, followed by an acknowledgment.

BF frames. The beamforming training is carried out using BF frames which is a type of control frame. The BF frame consists of a preamble, a header, and a payload as shown in Fig. 2. Both beacons and sector level sweep (SLS) frames are referred to as BF frames because they are sent out in all sectors by the AP, and can be used for backscatter in mm-Comb. The preamble consists of 59 repeated Golay sequences $(Ga_{128}, Gb_{128}, -Ga_{128}, \text{ and } -Gb_{128})$, while the header and

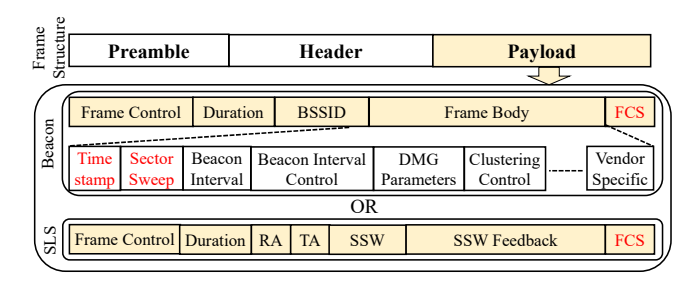


Figure 2: 802.11ad beamforming (BF) frame.

payload are spread with Ga_{32} where the subscript represents the length of sequence. Most of the fields in the BF frame are predetermined and remain constant, except for the timestamp, sector sweep field, and FCS (frame check sequence) marked in red in Fig. 2. The BF frames are transmitted in different sectors during the BF training. The BF frame's data rate is 27.5 megabits per second, coded with an LDPC code at a 1/2 coding rate, and each coded bit is then spread using a 32-point length Golay sequence, producing symbols at a rate of 55 MSym/s at a chip rate of 1760 MHz.

3 mmWave WiFi Backscatter

This section explains how the mmComb tag inserts backscatter bits into ongoing mmWave WiFi frames and how a commodity mmWave WiFi device retrieves these bits through demodulation.

3.1 Modulation and demodulation

Modulation. Our objective in mmComb is to reuse the existing mmWave WiFi frames as a query signal for the backscatter tag. However, reusing any arbitrary frame makes it difficult to isolate backscatter bits from the original frame's bits, as both are unknown to the receiver. Prior work on sub-6 GHz commodity WiFi backscatter [53,54] relies on separating the two in the frequency domain by shifting the backscatter signal to an adjacent WiFi channel. Albeit effective, this process is not feasible in mmWave WiFi where each 802.11ad/ay channel is 2.16 GHz wide, and shifting to adjacent frequency will require a power-hungry high-speed oscillator on the tag.

In order to address this challenge, mmComb utilizes 802.11 ad/ay BF frames. As described in Sec. 2, most bits of 802.11 ad/ay BF frame are fixed. Since 802.11ad/ay BF frames adopt DBPSK modulation, mmComb embeds backscatter bits onto the BF frames by changing the symbol phase according to them. This is demonstrated in Fig. 3. A mmComb tag

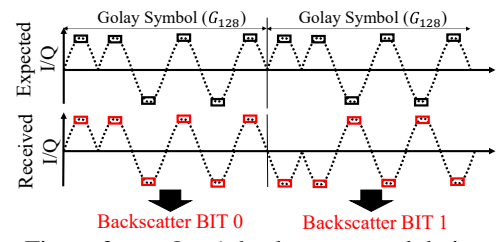


Figure 3: mmComb backscatter modulation.

backscatters the incoming WiFi signal with an offset of either

 0° (backscatter bit 0) or 180° (backscatter bit 1). Here, the reflected symbol $S_{\text{reflected}} = S_{\text{original}} \times e^{j\pi b_{\text{back}}}$ where S_{original} is the original incoming symbol and b_{back} is the backscatter bit to be embedded. This means that if the backscatter bit is 0, the signal has no change, and if the backscatter bit is 1, the original signal is phase-shifted by π before backscattering. Our backscatter data rate of 55 Mbps is achievable due to a symbol rate of BF frames (55 MSym/s).

To create a phase shift, we develop a tag that uses a Single Pole, Double Throw (SPDT) switch with one input port and two output ports as shown in Fig. 4. The WiFi signal enters

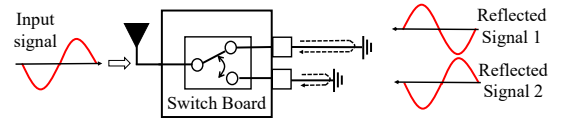


Figure 4: mmComb tag schematic: by switching between the output ports, the tag can reflect with different phases.

the input port and bounces back through one of the output ports. The output ports create different phase shifts due to the different lengths of lines, resulting in a quarter wavelength discrepancy between them. This leads to a half wavelength difference, or a phase shift of π , during a complete round trip. By switching between the output ports, the reflected signal can be modulated with two different phases. mmComb uses a high-speed SPDT switch with 100 MHz of switching speed and 1ns rise and fall times (more details of the prototype in Sec. 5).

Demodulation. An 802.11ad/ay receiver can now demodulate the backscatter bits by comparing expected and received signals. The received signal y(t) is a linear combination of the transmitted signals from K different paths as

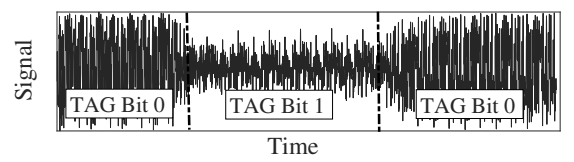
$$y(t) = A(\theta_b) \cdot h_b(\theta_b) \cdot e^{j\pi b(t)} \cdot s(t) + \sum_{i=1, i \neq b}^{K-1} A(\theta_i) \cdot h_i(\theta_i) \cdot s(t)$$

where $A(\theta_i)$ and $h(\theta_i)$ are the complex antenna weight vector and channel gain in direction θ_i , respectively. s(t) is the transmitted signal, and θ_b and b(t) represent the angle of the backscatter path and backscatter bits, respectively.

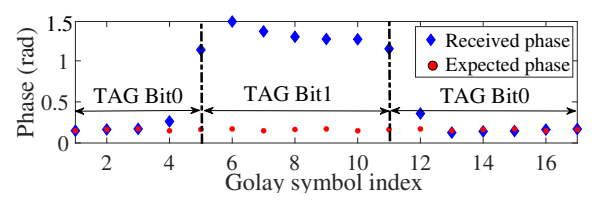
Typically when a frame is transmitted, the receiver first estimates the channel using the channel estimation field (CEF) and uses the estimated channel to demodulate the transmitted signal. In the case of mmComb, with the use of BF frames, s(t) is already known to the receiver, enabling us to solve for b(t) to extract the backscatter bits.

To achieve this, mmComb tag creates no phase change (i.e., backscatter bit b(t)=0) during the CEF of the BF frame, resulting in the receiver being able to estimate $H=A(\theta_b)\cdot h_b(\theta_b)+\sum_{i=1,i\neq b}^{K-1}A(\theta_i)\cdot h_i(\theta_i)$. This channel estimation and known s(t) can be used to estimate the expected received signal $y_e'(t)$ at the receiver. That is, $y_e'(t)$ represents the case of a signal received by the receiver without being changed by the tag. The backscatter bit b(t) can then be extracted by comparing the received signal y(t) and the estimated signal

 $y_e'(t)$. If the different $y - y_e'$ is zero, the backscatter bit b(t) = 0. On the other hand, if the difference becomes $2 \cdot A(\theta_b) \cdot h_b(\theta_b) \cdot s(t)$, the backscatter bit b(t) = 1. Fig. 5 shows an example of expected and received signals and corresponding backscatter bits. In practice, the difference might vary from $2 \cdot b$



(a) Raw signal of 802.11 ad golay symbol.



(b) Phase shift due to tag operation.

Figure 5: Embedded backscatter bit on the Golay symbol. $A(\theta_b) \cdot h_b(\theta_b) \cdot s(t)$ and we use a threshold which is the mean difference over the frame for determining the backscatter bit. **Embedding backscatter frame.** Fig. 6 shows our mmComb backscatter frame is embedded inside the 802.11ad/ay frame. Since the length of the BF frame is fixed, the backscatter frame size can also be predetermined including the size of the preamble and data. The *B-preamble* provides synchroniza-

Preamble	Header	Payload							
Time Stamp B-P	reamble	B-Payload							

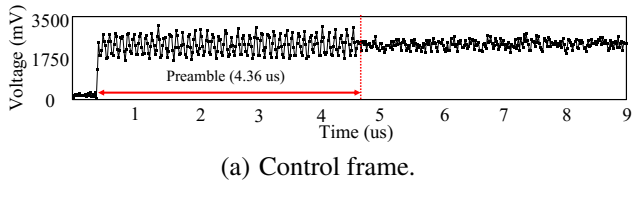
Figure 6: The backscatter frame (B-preamble & B-payload) can be embedded inside the 802.11ad/ay frame.

tion to indicate the start of the backscatter frame. We note that the *B-preamble* must be inserted after the timestamp of the BF frame body at 11.58 μs (4.30 μs of preamble, 4.67 μs of header, 1.45 μs of frame control, duration, and BSSID, and $1.16 \,\mu s$ for timestamp). Since our tag demodulation is based on comparing the original bit sequence with the changed one, it is essential that the tag bit flips occur only after the timestamp. Although it is possible to embed backscatter data even before the timestamp, 802.11ad/ay frames scramble the bits, and any modification to the timestamp because of backscatter data can result in incorrect descrambling. Since mmComb relies on fixed data of the BF frame, proper descrambling is essential to extract the backscatter bits. The backscatter frame can be of length $(L-11.58) \mu s$ where L is a length of the original BF frame, leading to $\lfloor \frac{(L-11.58)*1000}{55} \rfloor$ backscatter bits per BF frame.

3.2 Ultralight DMG control frame detection

A natural challenge that arises in using a DMG BF control frame is that a tag needs to respond only to a control frame.

In order to determine the type of 802.11ad packet, it is necessary to demodulate the packet from the tag. However, this is not possible under a limited power budget, as demodulation requires a mixer and a high-speed oscillator. Instead, there are two distinctive aspects to the control frame: 1) the preamble sequence (repeated Gb_{128} symbols) remains highly correlated after passing through a narrow bandwidth filter; 2) the control frame (48 Gb_{128} symbols) has a longer preamble than the data frame (16 Gb_{128} symbols), and this observation allows the tag to detect the type of frame without adding complex hardware. The type of frame is detected using a power detector. A power detector is a powerless device that simply converts received RF signals into voltages without consuming power.



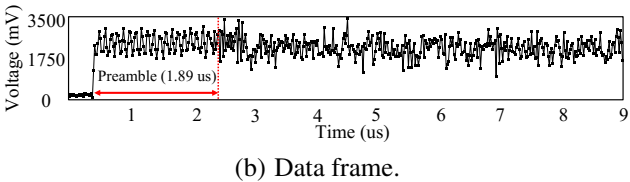


Figure 7: A control frame and a data frame captured by a power detector with a sampling rate of 55 MHz.

Interestingly, a narrow 10MHz bandwidth (about 0.4% of 2.17 GHz) still shows a high correlation for the power detector's output voltage during the preamble due to the redundancy of the repeated Gb_{128} symbols. Although the detector's narrow bandwidth causes signal distortion, we observe high similarity between successive distorted Golay symbols. Using this, it is possible to detect a control frame in a tag efficiently without a complicated demodulation process and hardware. Fig. 7(a) and Fig. 7(b) show the output voltage of the power detector for a control frame and a data frame, separately. It's worth noting that there is a clear difference between control frames and data frames. This is due to the fact that a control frame utilizes a Golay sequence that spreads both the preamble and the payload, whereas only the preamble field in a data frame uses a Golay sequence. Leveraging its unique property, mmComb tag calculates the auto-correlation of output voltage on distorted Golay symbols using a sliding window. The correlation output can detect both the start and type of a frame.

As shown in Fig. 8, a high correlation is observed throughout the entire control frame, while the correlation drops after the preamble in the data frame. Using a threshold-based cutoff, we can detect the type of frame with 98.5% sensitivity $(\frac{TP}{TP+FN})$ and 99.1% accuracy. The detection can be completed in $\approx 2\mu s$ as the length of the data frame preamble is only $1.89\mu s$.

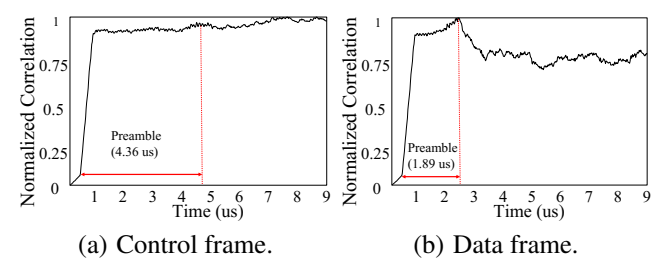


Figure 8: The correlation outputs differ between a control frame and a data frame.

4 Suppressing Self-interference

While the mmWave commodity backscatter techniques described in the previous section ensure proper modulation, demodulation, and embedding of the backscatter bits, high self-interference can result in low backscatter SINR. Here, the self-interference refers to all incoming signals received directly from the AP to the client, including LoS and NLoS paths, but not the backscatter path.

As mentioned earlier, shifting the center frequency of the backscattered signal is not feasible for wide 802.11ad/ay WLAN channels due to a limited power budget. Instead, we exploit the directionality of mmWave communication to separate the backscatter and self-interference signals in the spatial domain through careful beamforming and nulling. Our main objective here is to identify a *receiver beam antenna weight vector* that maximizes the gain towards the backscatter tag while creating the nulls in the direction of self-interference. This is demonstrated in Fig. 9. Apart from improving SINR, a

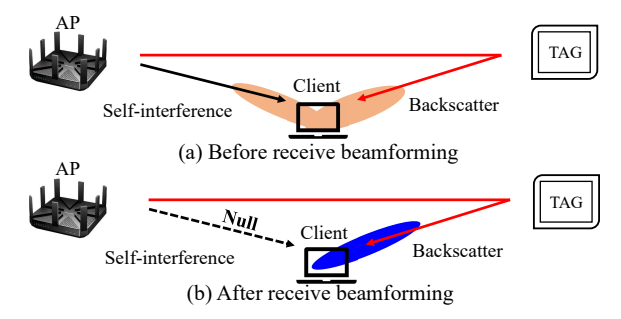


Figure 9: Our receive beamforming creates a custom beam with high gain towards the tag and nulls towards the self-interference to improve backscatter SINR.

key advantage of this design is that it offloads the responsibility of self-interference mitigation on the receiver (a commodity device) without adding any complexity to the tag design.

Such beamforming and nulling require us to address the following questions: (i) how can we determine the backscatter path in a composite signal received at the receiver, which also includes self-interference signals? (ii) how can we estimate the angle of arrival (AoA) for the backscatter and self-interference paths? (iii) how can we create a beam towards the tag direction and nulls towards self-interference directions using the AoA information when both signals are highly correlated? and lastly, (iv) how can we develop a backscat-

ter protocol that is compatible with commodity mmWave devices?

4.1 Backscatter beamforming with nulling

In this section, we first address how to create a high-gain beam towards the tag while nulling the self-interference.

Beamforming primer. Beamforming is achieved through a weight vector applied to antenna elements in mmWave's phased antenna array. This creates varying phases and amplitudes in incoming or outgoing signals. Fig. 10 shows the receive beamforming. Each antenna element receives the sig-

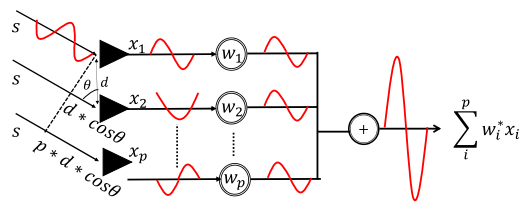


Figure 10: Illustration of beamforming.

nal with a different phase value, also known as the steering vector, depending on the angle of arrival (AoA). This can result in a decrease in signal strength due to destructive interference between received signals from each antenna element. To address this concern, each element is assigned a weight based on the AoA to enhance signal strength and improve performance, ensuring that signals are received with high SNR. If the transmitted signal s(t) arrives at the receiver with an incident angle of θ_k for the k^{th} path, the received signal becomes $x(t) = s(t) * a(\theta_k)$ where $a(\theta_k)$ is the steering vector for p antenna elements. $a(\theta_k)$ is essentially a vector of phase shifts τ_k introduced by different travel lengths for different antenna elements and can be written as $a(\theta_k) = \{1, e^{\tau_k}, \dots, e^{(p-1)\tau_k}\}, \quad \tau_k = \frac{-j2\pi f_c dcos\theta_k}{c}$ where d, c, and f_c are the spacing between adjacent antenna elements, the speed of the light, and the center frequency, respectively. When there is only a single path (k = 1), the weight vector can be calculated by compensating for the additional phase shifts for that path, i.e., $w(\theta_k) = \{1, e^{-\tau_k}, \dots, e^{-(p-1)\tau_k}\}$. When there is more than one path, the weight vector should depend on the steering vector matrix $A = [\sum_{j=1}^{k} a_1(\theta_j), \dots, \sum_{j=1}^{k} a_p(\theta_j)]$ for all incoming paths, i.e., $w = [\sum_{j=1}^{k} w_1(\theta_j), \dots, \sum_{j=1}^{k} w_p(\theta_j)]$. However, when the incoming signal contains both the desired signal and the self-interference as in mmComb, it is non-trivial to find the weight vector that maximizes only the backscatter signal while nulling the self-interference.

Beamforming for backscatter only. mmComb creates the optimal weight vector by calculating a covariance matrix using the AoA information. This method provides an approach that can be readily implemented without any protocol modifications or additional measurements. Existing works such as [13,26] propose to use evolutionary algorithms or neural networks for estimating the optimal weight vector. They then use multiple SNR measurements to evaluate the fitness of the estimated solution. However, in our case, both the backscatter and self-interference signals are strongly correlated (they are

simply a phase-shifted copy of each other) which makes it difficult to use the SNR measurements for the fitness evaluation. mmComb utilizes spatial smoothing technique to decorrelate incoming signals to find the optimal weight vector. We now describe the optimal weight vector calculation process adopted for our scenario.

For ease of exploration, let us consider a linear antenna array with p elements receiving signals. The received signal y is then represented by $y = \sum_{i=1}^p w_i^* x_i = w^* x$ where x and w are the received signals and weight vectors, respectively, and * indicates complex conjugate transpose of vectors like in Fig. 10. As we described in Sec. 4.2, we can differentiate between backscatter and self-interference paths and calculate their AoA. This can enable us to calculate the optimal weight vector. Specifically, if the ideal received signal (i.e., only the backscatter signal) from the backscatter path is y_b , we can nullify the self-interference by minimizing the error $\varepsilon = y - y_b = w^* x - y_b$ between the received signal and the ideal backscatter signal. The mean squared error $E[\varepsilon \varepsilon^*]$ can be calculated as

$$E[\varepsilon \varepsilon^*] = E[(w^*x - y_b)(w^*x - y_b)^*]$$

= $w^*Rw - 2w^*r + y_b * y_b$ (2)

where $R=E[xx^*]$ is the auto-correlation of the signal arriving at each antenna element and $r=E[y_bx^*]$ is the cross-correlation between the ideal backscatter signal and arrived signal. By finding the minimum using differentiation $\frac{dE[\epsilon\epsilon^*]}{dw}=2Rw-2r$, we can get the optimal weight vector $w=R^{-1}r$. Intuitively, R^{-1} cancels the self-interference signals and r creates a high-gain beam towards the backscatter direction. We calculate the y_b and x by replacing the desired signal and interference signal with the steering vectors from their AoA. Therefore, y_b can be the steering vector of a tag direction while x is the steering vector of the combined signal. We then use them to calculate the optimal weight vector.

There is, however, a critical challenge in simply adapting the correlation matrix to determine the optimal vector. The matrix calculation assumes that the incoming signals of backscatter and self-interference are mutually not correlated. If the signals are coherent, there will be a rank loss in the covariance matrix [10], resulting in the creation of wrong weight vectors.

Spatial smoothing for phased arrays. To address the challenge, we leverage a unique characteristic of mmWave WiFi that has a large number of antenna elements to decorrelate the incoming signals. Using this redundancy of these antenna elements, mmComb applies the spatial smoothing technique by splitting the array into several subarrays [40]. This is shown in Fig. 11. Spatial smoothing has been used for decorrelating signals in the context of AoA estimation [20, 48]. In order to accurately estimate the Angle of Arrival (AoA), it is important to identify the Eigenvector of the steering vectors for incoming signals. These vectors need to be orthogonal to each

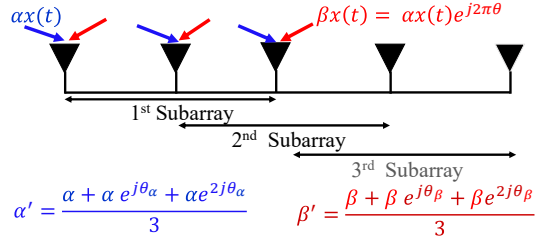


Figure 11: Spatial smoothing: The correlated incoming signal α and β become decorrelated signal α' and β' .

other. However, if the incoming signals are correlated, they lose their orthogonality even if they have different AoAs. To overcome the issue of correlated signals, as shown in Fig. 11, the incoming signals are averaged over the subarrays to decorrelate them.

Let us assume that L subarrays are created from the p antenna elements where each subarray size is M. This yields L=p-M+1. Let $x_i(t)=AD^{i-1}s(t)$ denote the received signal at the i^{th} subarray where A is the steering vector for the subarray. A is $M\times K$ Vandermonde matrix with rank K (number of paths). D is K dimensional diagonal matrix of K paths' AoA ($D=diag\{e^{-j\omega_0\tau_1},\ldots,e^{-jf_c\tau_k}\}$). Then the correlation matrix of the i^{th} subarray is represented by $X_i=E[xx^*]=E[(A_MD^{i-1})S)(A_MD^{i-1})S)^*]=A_MD^{i-1}SD^{*(i-1)}A_M^*$ where S is the correlation matrix of the transmitted signal ($S=E[s(t)s(t)^*]$). If there are L subarrays, the smoothed covariance matrix becomes the mean of the subarray covariances which can be presented as

$$\overline{X} = \frac{1}{L} \sum_{i=1}^{L} X_i = A \left(\frac{1}{L} \sum_{i=1}^{L} D^{(i-1)} S D^{*(i-1)} \right) A^* = A \overline{S} A^*$$
 (3)

where \overline{S} is the modified signal source and is non-singular even with coherence signals given that $L \geq K$. As an example, with our commercial mmWave WiFi hardware, the 6×6 phased array can be configured as 4 subarrays of 5×5 as shown in Fig. 12(a). We then average the measured power delay profile over the subarrays of the antenna so that the signals from different directions become decorrelated signals. Figs. 12(c)-12(e) show the impact of spatial smoothing on an example beam pattern with and without nulling.

4.2 Extracting the backscatter path

To achieve the above-mentioned beamforming with nulls, we need to identify the backscatter path(s) and self-interference path(s) along with their AoA. Although mmWave channel sparsity (3-4 paths in typical indoor environment [49]) reduces the complexity of the problem, It is difficult to distinguish between the backscatter signal and the self-interference signal as they are the same signal but with different channels. We adopt a power delay profile (PDP) based solution for estimating AoA. Specifically, we leverage the approach proposed in [43] for beam alignment and [34] for localization. A detailed description of the AoA estimation method can be found in Appendix A1.

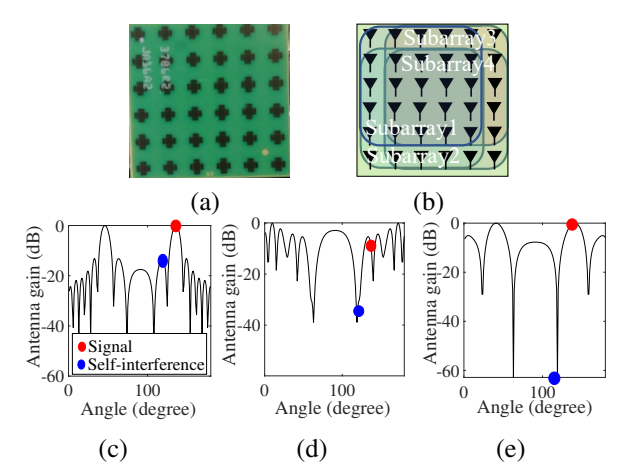


Figure 12: (a) 6×6 phased array used in 802.11ad devices and (b) spatial smoothing with L=4; Example beam patterns of (c) without both nulling and smoothing, (d) with nulling and without smoothing, (e) with both nulling and smoothing

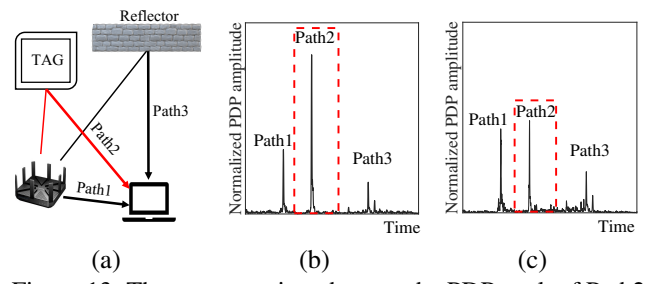


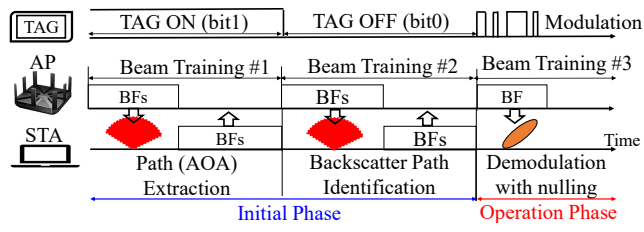
Figure 13: The tag operation changes the PDP peak of Path2.

Identifying the backscatter path. After determining the AoA of different paths, we need to classify them as either backscatter paths or self-interference paths. We leverage a simple observation: during the tag operation, only the amplitude of the backscatter path changes, not the self-interference (LoS and ambient reflections) paths. Fig. 13 shows measured PDP for one backscatter path and two self-interference paths.

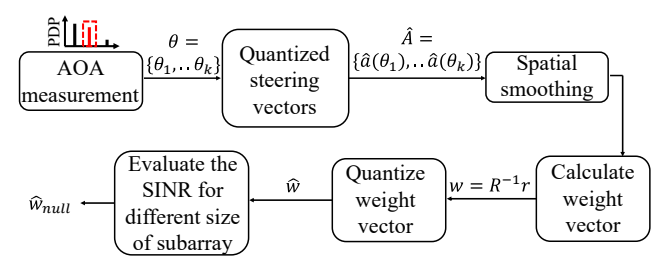
4.3 mmComb backscatter protocol

We now discuss how mmComb can operate with 802.11ad/ay protocol without any protocol modification. Our system operates as shown in Fig. 14(a).

The AP periodically exchanges BF frames with a client (STA) to maintain the link between the AP and the STA. Note that while we refer to this as beam training here which is typically accomplished through SLS frames, a round of beacons sent out by the AP can also be used for the purpose as mentioned in Sec. 2. During the initial phase, the tag operates as ON (bit 1) for the first beam training and as OFF (bit 0) for the second beam training. The initial phase helps the client receiver extract all paths, identify the backscatter path, and estimate the AoA for the backscatter and self-interference paths. Although AoA estimation requires 2 beamforming training, only one measurement is needed for starting backscattering communication. This is followed by a procedure at the client where quantized steering vectors are calculated, spatial



(a) mmComb over 802.11ad/ay.



(b) Steps in beamforming vector calculation with nulling Figure 14: mmComb framework.

smoothing is applied, and the weight vector that provides the best SINR is selected, as shown in Fig. 14(b). Through this process, the client receiver determines a custom beam that can provide high SINR for backscatter communication. The AP sends out BF frames in different Tx sectors, modulating them with tags. The receiver then demodulates the backscatter data using a custom receive beam. In case of a channel change (for example, human mobility nearby), the AoAs can be recalculated. Fortunately, the channel change is also likely to trigger beamforming for the STAs in the network. This can be leveraged for quickly recalculating the AoAs to maintain a continuous backscatter connection. Therefore, there is a high chance that more than two beamforming opportunities are available within one beacon interval under frequent beamforming. This results in the initial phase being completed within one beacon interval, including path extraction which takes less than $300\mu s$ [43, 45]. We note that mmComb can leverage any control frame for piggybacking the backscatter data. Also, beamforming can occur multiple times within one beacon interval especially when multiple clients are connected to the AP. Both these factors greatly increase the opportunity to perform backscatter communications. Furthermore, the idea of mmComb is to integrate mmWave backscatter tags in the mmWave WLANs (just like conventional mmWave clients). So, it is possible that the AP uses additional beamforming frames to enable communication with the tags.

This protocol also holds for multiple tag cases. Due to the channel sparsity of mmWave, only a few tags respond in each sector (i.e., have high gain for incoming signal). Additionally, due to the different traveling distances, different tags can be differentiated as separate peaks in PDP (Fig. 13), allowing the receiver to determine the AoA for each tag. With this given AoA information, a receiver can perform Rx beamforming for a specific tag while nulling other tags that can respond to the same Tx sector. We further demonstrate this in Sec. 6.4.

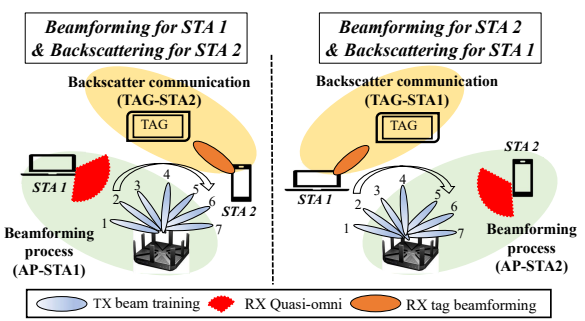


Figure 15: Illustration of mmComb protocol

One potential issue is that when a station (STA) acts as a receiver (Rx) for backscatter and changes its receive beam from quasi-omni to a new customized beam, it may provide the AP with an inaccurate sector (the highest SNR sector from the AP to the STA) during the process of beamforming (Fig. 1). We have observed that this problem does not arise in our system. The reason behind this is that when an STA performs beamforming with the AP, it doesn't allow backscatter communication to prevent any interference with its beamforming process. Instead, the STA acts as the Rx for a backscatter when the AP is performing beamforming with other STAs. This is demonstrated in Fig. 15 using one AP and two STAs. During beamforming training with STA1, the AP can utilize STA2 as a receiver for a backscatter tag. In this process, the tag uses BF frames from the AP to backscatter data to STA2, received over a custom beam with self-interference nulling. The STA1 receives AP's BF frames in quasi-omni mode as per protocol while maintaining unaffected communication with the AP. The beamforming training for different stations is conducted by the AP in separate time slots. Hence, the same is true when the AP performs beamforming with STA2 and STA1 receives the backscatter signals.

5 Implementation

5.1 mmComb Tag Prototype

Our tag prototype is shown in Fig. 16. We fabricated four prototype tags with a GotMIC gSSD0011 SPDT switch that is attached to the housing using a conductive epoxy and packaged with gold-plated aluminum. The switch can support switching speeds up to 100 MHz with rise and fall times of up to 1ns. The return loss (S_{11}) of the tag is measured and shown in Fig. 16(c).

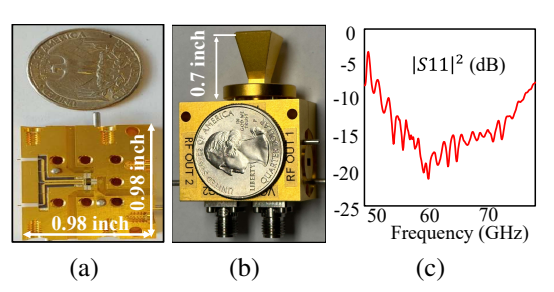


Figure 16: (a-b) Our mmWave tag prototype, (c) S(11) return loss measurements of our tag.

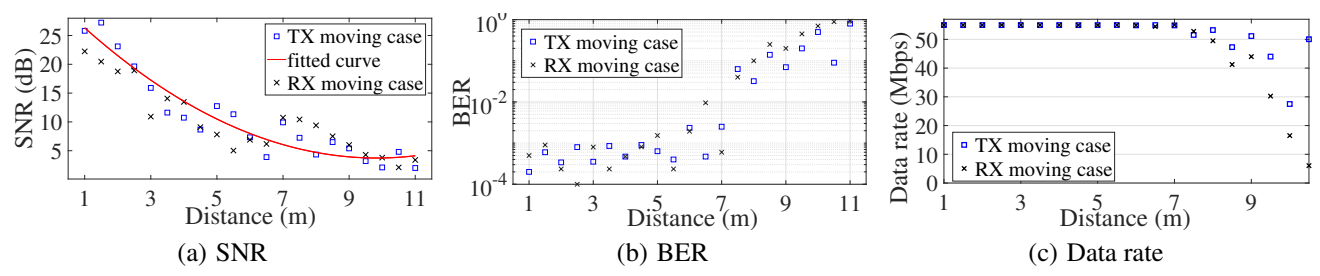


Figure 17: Backscatter SNR, BER, and data rate at different distances.

mmComb tag attaches a tag antenna (15 dBi V-band antenna SAR-1532-15-S2 with a half-power beamwidth of 41 degrees) to absorb or reradiate a backscatter signal. The tag output ports are attached to reflective ends where one of them reradiates the received signal without any change and the other introduces a phase shift of π using an additional round-trip of quarter wavelength. The switch is controlled through a TerasIC FPGA board with a microcontroller (SAM4SD32C).

5.2 mmComb Commodity WiFi Readers

Commodity 802.11ad devices from Airfide [4] and Mikrotik [2] are used as commodity readers in mmComb, as they use the same 802.11ad Qualcomm QCA6310 chipset and 6×6 antenna array. To enable desired modifications, we implement various changes to the 802.11ad Wil6210 driver and firmware to (i) send BF frames to selected sectors as desired, (ii) set selected Tx and Rx beams, (iii) extract per-element CSI (amplitude and phase), and (iv) create and apply new codebook to firmware with desired weight vectors.

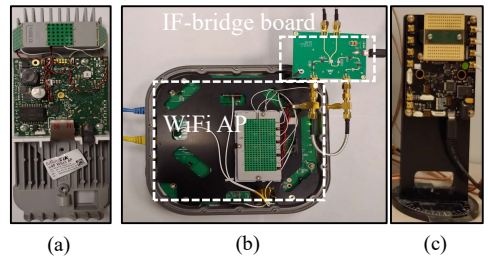


Figure 18: mmComb uses 802.11ad APs as Tx with two types of Rx: (a) 802.11ad MikroTik AP TX, (b) Airfide AP RX with IF bridge board, and (c) SiversIMA 60 GHz RF SDR RX.

We consider two types of setup: (i) both Tx and Rx are commodity 802.11ad devices, and (ii) the Tx is a commodity 802.11ad device while the Rx is a 60 GHz SDR. In both setups, the Tx transmits 802.11ad BF frames. The first setup includes two types of commodity receivers: an unmodified commodity 802.11ad device and a commodity 802.11ad device equipped with an IF bridge board [57] to extract raw I/Q data as shown in Fig.18. The unmodified 802.11ad receiver allows for commodity compatibility, demonstrating that backscattered beamforming frames can be received without any modifications to hardware, software, or protocol. In contrast to the prior work such as [53] where the checksum errors are ignored (through driver/firmware modification in

sub-6 GHz WiFi), we note that the current and only publicly available 802.11ad firmware (wil6210) internally drops the frames with a checksum error. To avoid it, mmComb tags further modulate the checksum (Sec. 2) based on the modified data so that the frame can be correctly received on an unmodified 802.11ad Rx. However, it only evaluates frames correctly received at the Rx and does not allow accurate calculation of BER. In order to evaluate it even on low SNR scenarios where the frame cannot be correctly received by the firmware, we use the IF bridge board on 802.11ad Rx to extract the raw I/Q data. The raw bits are decoded and analyzed with Keysight's 81199A Wideband Waveform Analyzer. We note that the IF bridge board is only used on the Rx for detailed bit-level analysis of backscatter BF frames. Our proposed design works with an unmodified 802.11ad Rx without the IF bridge board as we show in Fig. 21.

In the second setup, we use SiversIMA 60 GHz RF frontend with a 16-element phased array on the Rx. Compared to the phased array found in commodity 802.11ad devices which provides 2-bit phase control, the SiversIMA array provides 6-bit phase control, enabling us to better analyze the impact of beamforming and nulling on backscatter BER. Since most antenna arrays used COTS 802.11ad devices do not provide per-element amplitude control, we also focus only on phase control in this work.

6 Evaluation

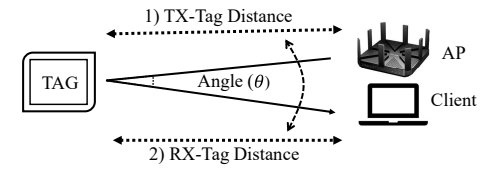
We perform exhaustive experiments to evaluate the performance of mmComb under diverse scenarios. They include (i) benchmarking read range and angles, (ii) commercial device FRR, (iii) nulling performance and impact on BER, (iv) NLoS situations in practical deployments, (v) impact of tag on mmWave WiFi, (vi) multiple simultaneous tags, and (vii) power consumption.

6.1 mmComb read range and angle

Backscatter range. We first perform a micro-benchmark for mmComb read range in a $12m \times 12m$ office room. The setup is shown in Fig. 19(a) where 802.11ad devices are used as Tx and Rx. The tag and one endpoint (either Tx or Rx) are stationary while the other endpoint gradually moves to increase distance. This is a common scenario in mmWave WLANs, where an AP (Tx) is fixed and a client (Rx) is located at varying distances from the tag. The Rx captures the modulated 802.11ad BF frames sent by the Tx AP. These

frames are then analyzed to determine the backscatter SNR and BER. Figs. 17(a) and 17(b) show the mean SNR and BER for different distances. We find that even up to 5.5m distance, the BER remains below 10^{-3} . Even for a range of 7m, the BER remains lower than 10^{-2} . Fig. 17(c) shows that mmComb achieves a data rate of 54.4 Mbps up to 7m (out of the maximum possible data rate of 55 Mbps).

Impact of angle. Unlike legacy WiFi, mmWave WiFi is highly susceptible to angular changes due to directionality. As shown in Fig. 19(a), we set a tag at 2m distance from the



(a) Setting for tag angle & distance evaluation.

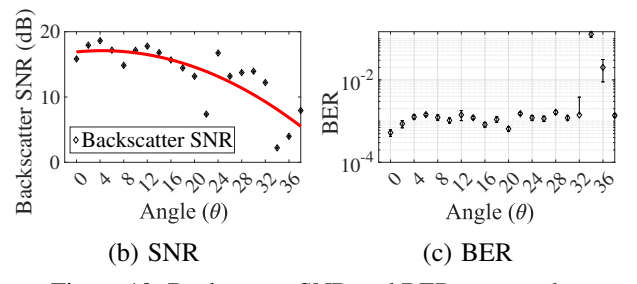


Figure 19: Backscatter SNR and BER over angle.

802.11ad devices and increase the angle from 0° to 38° . Here, the Rx position is fixed as it utilizes a beam pattern to receive the signal from the tag, while the Tx position is changed to vary the angle. As observed in Fig. 19(b), the backscatter SNR remains higher than 7.9 dB even for 38° which is close to the antenna beamwidth of 41°. Fig. 19(c) shows that the mean BER remains lower than 1.3×10^{-2} over all angles within the tag antenna beamwidth.

Tag at different locations. We conduct an experiment by varying the incident angle of the backscattered signal to Rx. Fig. 20 shows a $10m \times 10m$ room where we perform over 200 measurements at 20 different locations. These locations

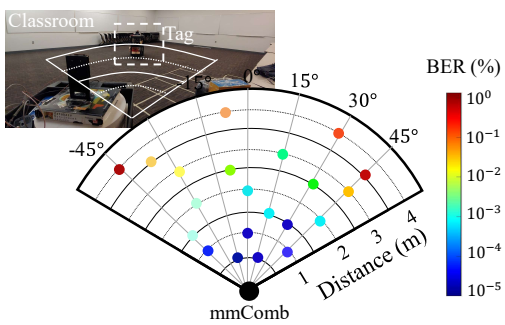


Figure 20: Backscatter BER for 20 different tag positions

are randomly chosen to create different incident angles and distances. The position of Tx and Rx devices are fixed while the Rx performs beamforming towards the tag (as well as nulling for self-interference) depending on its position. The incident angle is varied from -45° to $+45^{\circ}$. As we can see in Fig. 20, we can achieve consistently low BER over the 90° span and up to 4m distance.

Frame reception ratio. We now use the 802.11ad MikroTik devices as both Tx (AP) and Rx (client). We deploy the two in a $12m \times 12m$ classroom along with a tag that backscatters by modulating the BF frames sent by the AP. As mentioned earlier in Sec. 5.2, the tag not only modulates the BF frame body part but also the checksum, making it possible for the unmodified commodity Rx to receive the frame. Since the received frame is processed through the (closed source, proprietary Wil6210) firmware, we directly measure the frame reception ratio (FRR) at the Rx along with SNR. To collect the SNR from commercial devices, we utilize the SNR report from feedback frames. In the BF process, the SSW feedback frames report the client's observed SNR back to the AP. The measured SNR is reported as 8-bit two's complement value of $4 \times (SNR - 19)$). The Rx extracts backscatter data by comparing known/expected BF frame bits with received ones. Fig. 21

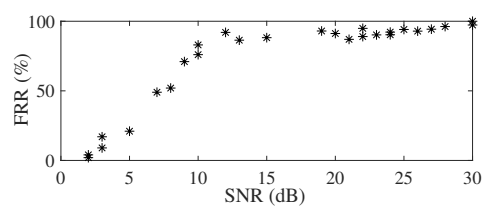


Figure 21: Frame Reception Ratio

shows the FRR for different SNR values. Similar to previous results, when Rx performs beamforming toward the tag to achieve a high gain (SNR ≥ 10 dB), the average FRR is observed to be 91.4%.

6.2 Nulling backscatter self-interference

In this section, we evaluate how mmComb's beamforming with self-interference nulling performs. To do so, we perform extensive experiments to analyze: (i) the creation of custom beams with nulls, (ii) the impact of phase resolution, (iii) the subarray size in spatial smoothing, (iv) nulling with multiple nulls, (v) performance comparison with state-of-the-art nulling techniques, and (vi) different mmWave WiFi devices.

Creating beam patterns with nulls. To understand the nulling performance, we place the tag at arbitrary locations. The identification of the path and estimation of AoA are performed for backscatter and self-interference paths. We then compare two types of beams - one that is chosen directly from the codebook without any self-interference nulling and another one that uses mmComb nulling. Fig. 30 in Appendix A2 shows examples of six beam patterns before and after nulling with 4-bit phase resolution. The receiver was mechanically rotated while the transmitter sent signals over the LoS path to measure beam patterns. As shown in Fig. 22(a), the nulling performance can be calculated by subtracting the gain of the main lobe in the backscatter direction from the gain of the

null in the self-interference direction. The results indicate an average nulling performance of 27.6 dB, with a maximum of 33.4 dB. Compared to the default beam pattern in the codebook, our nulling results in an average gain of 19 dB, but it reduces the gain of the main lobe to an average of 1.95 dB.

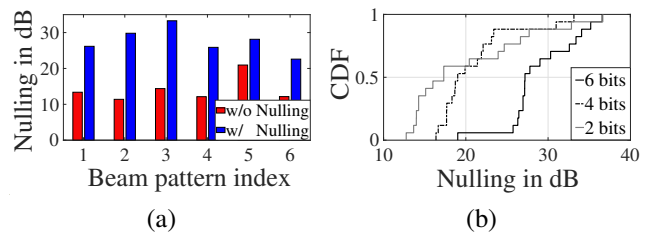
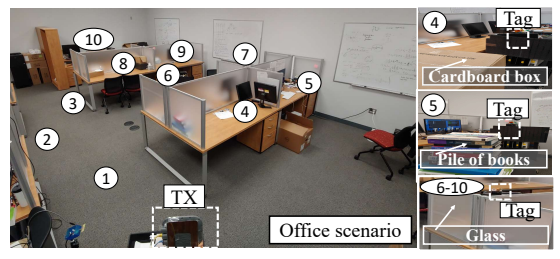
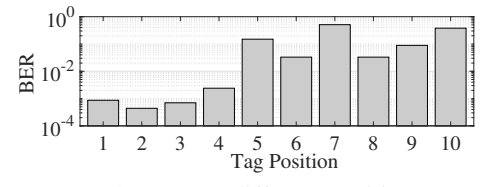


Figure 22: Nulling performance for (a) 6 beam patterns shown in Fig. 30 and (b) 25 beams with different phase resolution.

Impact of phase resolution. Given that today's mmWave WiFi antenna arrays offer low phase resolution, we compare nulling performance at 25 different tag locations (different directions of backscatter and self-interference) for 2-bit, 4-bit, and 6-bit phase resolution. The results are shown in Fig. 22(b). We find that over 50% of measurements achieve nulling performance of 27.2 dB or higher with a 6-bit resolution. The performance degrades with a coarser resolution of phase control as we expected. However, the mean nulling performance is still 20.1 dB and 20.9 dB for 2-bit and 4-bit resolution, respectively. Additional evaluations for nulling (different devices, number and size of subarray in spatial smoothing, and multiple self-interference paths) can be found in Appendix A2.



(a) Evaluation for LoS (1-3) and NLoS (4-10).



(b) BER at different positions

Figure 23: mmComb performance in LOS and NLOS cases

6.3 Practical deployment

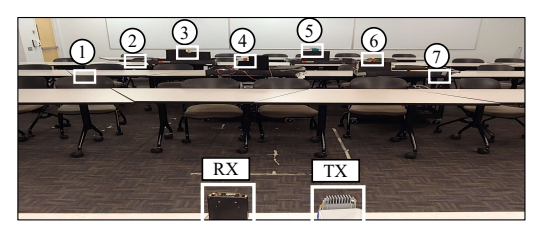
We now evaluate a practical scenario where the tags are deployed in an office environment (a $10m \times 10m$ room) as shown in Fig. 23(a). We deploy an Airfide 802.11ad AP in the corner of the room. The AP transmits BF frames across 36 different sectors. The 802.11ad clients are receivers placed in various

cubicles. The Fig 23(a) shows ten different tag positions. Positions (1-3) have a LoS path with the AP. The remaining positions (4-10) have blockage (cardboard boxes, books, etc.) and the signal either is received after penetration or reflection (NLoS) from nearby objects.

Fig. 23(b) shows the BER for 10 tag locations. We find that BER for positions 1-3 is less than 10^{-3} due to LoS (similar to Sec. 6.1). For NLoS cases, position 4 achieves low BER due to low penetration loss from the cardboard. The BER increases in positions 5-10 with books and glass blockages. Given that glass has a relative permittivity (ε) of 3.7 to 10 [19], the backscatter SNR drops. However, the corresponding average BER is still 2.1×10^{-1} . This is primarily due to the received beamforming towards the tag and self-interference nulling for other reflections in the room which significantly improves the SINR even when the incoming signal to the tag is weak.

6.4 Scalability of mmComb

We evaluate the scalability of mmComb with multiple tags and simultaneous operations. We create a scenario where we place tags at 7 positions in a $10m \times 10m$ classroom as shown in Fig. 24(a). We first operate the tags individually (with no other tag interference). Fig. 24(b) shows 10 Tx sectors (5 each



(a) Experiment setting for multiple tags.

	Single tag response				Two tags response			
TX sector	Tag Response	RX beamforming	Null for other tags	TX sector	Tag Response	RX beamforming	Null for other tags	
TX1	Tag3	Tag3	-	TX3	Tag1 & Tag4	Tag 1/4	Tag 4/1	
TX2	Tag2	Tag2	-	TX6	Tag2 & Tag3	Tag 2/3	Tag3/2	
TX4	Tag5	Tag5	-	TX8	Tag3 & Tag5	Tag 3/5	Tag 5/3	
TX5	Tag2	Tag2	-	TX9	Tag6 & Tag7	Tag 6/7	Tag 7/6	
TX7	Tagl	Tagl	-	TX10	Tag1 & Tag3	Tag 1/3	Tag 3/1	

(b) Tag response corresponding to a TX sector.

Figure 24: Multitag experiment.

for one and two tag responses) and the corresponding tags that can respond when a BF frame is sent in that Tx sector. We note that this setup uses a COTS 802.11ad AP as the Tx where the phased array antenna has non-uniform beam patterns with non-trivial sidelobes. This represents a real-world scenario and we anticipate the performance to be better (i.e., less inter-tag interference) when antenna arrays achieve a better directionality in the future. We observe that due to the directionality of Tx sectors, at most one tag responds in the majority (82.8%) of Tx sectors (not all Tx sectors are shown in Fig. 24(b)) even when they are densely deployed. In such cases, the Rx can beamform to the responding tag in each Tx sector to receive data from it in a time-divided manner (i.e., TDMA). We also observe that in a few Tx sec-

tors (17.2%), two tags respond. This is primarily attributed to the non-uniformity of Tx beams in today's phased arrays. As shown in Fig. 24(b), the Rx can beamform to one of the two tags and null to the other to reduce interference. Even with various randomly generated deployments in the presented scenario, we find that at most two tags respond in one Tx sector, requiring nulling interference from at most one tag at any time. We note that interference nulling through Rx beamforming is required only when two tags respond in the same Tx sector. It is not required if only one tag responds in a given Tx sector. When two tags respond in the same sector, the Rx can beamform to one and null to the other one by one in different beamforming rounds to receive data from both of them in a TDMA manner. To further validate this, we

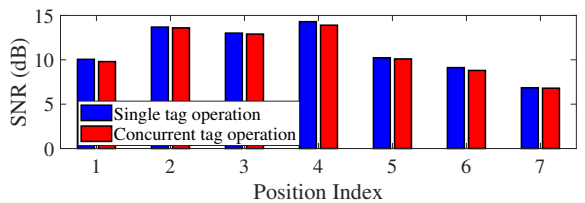


Figure 25: Single tag vs. concurrent multi-tag SNR. operate all seven tags in Fig. 24(a) simultaneously and use the TDMA-based tag communication for different Tx sectors and corresponding Rx sectors as shown in Fig. 24(b). Fig. 25 shows the difference between tags operating separately versus all tags operating concurrently. We find that even when the Rx does not perform nulling for other tags (e.g., TX1 or TX2) because only one tag responds in the Tx sector, concurrent operation of the other tags does not affect the SNR (an average SNR difference of only 0.2 dB). Similarly, when the Rx performs nulling (e.g., TX3 or TX6) in the case when two tags respond, the SNR difference between separate and concurrent operations is still very small (average 0.2 dB). Overall, these results show that mmComb can scale to multiple tags with backscatter communication happening in a time-divided manner (different tags readable in different AP sectors).

6.5 Power consumption

mmComb tag consists of four main components: clock, modulator, frame detector, and SPDT switch. We analyze the power consumption of the components using Libero SoC Smart-Power [24]. Serial inverters are used to generate a 55 MHz clock which is then input to the modulator and frame detector. The clock consumes $7.5\mu W$. The modulator provides control input to the switch for embedding backscatter bits in the signal and consumes only $2\mu W$. The frame detector module consumes 76.8µW and our GotMIC gSSD0011 SPDT switch only needs less than $1\mu W$ [14]. This results in total power consumption of $87.3\mu W$. This means that the tag can operate with a 1000mAh coin cell battery for over 4 years. Furthermore, it can operate battery-free using a solar cell which can harvest $100\mu W$ in a typically illuminated office environment [33].

Related Work

Conventional and sub-6 GHz WiFi backscatter systems.

Conventional backscatter systems such as UHF RFID have been studied for over two decades [11, 16, 30]. Compared to mmComb which can provide megabits per second data rates, these systems are primarily designed for low-power, low-rate reader-tag communication. High cost [12] of deploying dedicated readers has given rise to commodity WiFi backscatter systems. Such systems include WiFi backscatter [17], BackFi [7], Passive WiFi [18], Hitchhike [53] and WiTAG [3]. These systems are primarily designed for WiFi in sub-6 GHz bands.

mmWave WiFi and backscatter. mmWave backscatter systems have been recently proposed in [6, 28, 41]. Both [41] and [6] do not use WiFi commodity devices as readers but instead use FMCW radars. Apart from that, both works achieve limited data rates compared to mmComb. A highspeed mmWave backscatter system was proposed in [28] achieving a data rate of 100 Mbps. However, the proposed system requires additional hardware for a reader and a specialized antenna that can isolate backscatter signals using polarization. Extensive measurement studies have been conducted to understand 60 GHz links [36-38, 44, 49, 58] and interference [5, 31, 42, 52]. Creating nulls in the direction of interference has been studied in prior works including [15, 26, 29, 51]. Various novel types of algorithms including genetic algorithm [15, 26], BAT algorithm [47], Neural Network [13, 22] have been used to create antenna patterns with desired null behavior. The application of these algorithms poses several limitations in our case as the backscatter and self-interference signals are strongly correlated.

Conclusion and Discussion

In this paper, we introduced a 60 GHz mmWave WiFi commodity backscatter system. We believe that our work can be improved in three following aspects: (1) Tx beamforming: mmComb currently uses Rx beamforming at the client to receive data from the tag, while the AP utilizes unmodified codebook beams for BF frames. Incorporating TX beamforming along with RX beamforming can further reduce the selfinterference and improve backscatter SINR and BER. The Tx beamforming will also improve multi-tag operations by reducing inter-tag interference (i.e., improve TDMA) as Tx beamforming naturally assigns specific tags to different TX sectors under densely deployed multi-tag cases. Guaranteeing protocol compatibility with AP beamforming to the tags is a challenging issue that needs to be addressed in this context. (2) Tag antenna: An improved antenna design on the tag with a higher gain and wider field of view can help us further improve the backscatter SNR and BER. (3) Data rates: We note that our work only scratches the surface in terms of mmWave commodity backscatter. With an ample amount of available bandwidth, our work can be extended even further to achieve higher data rates while being commodity-compliant to realize the full potential of mmWave backscatter.

References

- [1] GLOBAL IOT CONNECTIONS TO HIT 29.4 BILLION IN 2030. https://transformainsights.com/news/global-iot-connections-294.
- [2] Mikrotik 60 GHz 802.11ad AP. https://mikrotik.com/product/wap_60g_ap.
- [3] Ali Abedi, Farzan Dehbashi, Mohammad Hossein Mazaheri, Omid Abari, and Tim Brecht. Witag: Seamless wifi backscatter communication. In *Proceedings of the Annual conference of the ACM Special Interest Group on Data Communication on the applications, technologies, architectures, and protocols for computer communication*, pages 240–252, 2020.
- [4] Airfide AFN2200. https://airfidenet.com/.
- [5] H. Assasa, S. Kumar Saha, A. Loch, D. Koutsonikolas, and J. Widmer. Medium access and transport protocol aspects in practical 802.11 ad networks. In 2018 IEEE 19th International Symposium on "A World of Wireless, Mobile and Multimedia Networks" (WoWMoM), pages 1–11, 2018.
- [6] Kang Min Bae, Namjo Ahn, Yoon Chae, Parth Pathak, Sung-Min Sohn, and Song Min Kim. Omniscatter: extreme sensitivity mmwave backscattering using commodity fmcw radar. In Proceedings of the 20th Annual International Conference on Mobile Systems, Applications and Services, pages 316–329, 2022.
- [7] Dinesh Bharadia, Kiran Raj Joshi, Manikanta Kotaru, and Sachin Katti. Backfi: High throughput wifi backscatter. *ACM SIGCOMM Computer Communication Review*, 45(4):283–296, 2015.
- [8] Spyridon-Nektarios Daskalakis, John Kimionis, Ana Collado, Manos M Tentzeris, and Apostolos Georgiadis. Ambient fm backscattering for smart agricultural monitoring. In 2017 IEEE MTT-S International Microwave Symposium (IMS), pages 1339–1341. IEEE, 2017.
- [9] Daniel Dobkin. *The rf in RFID: uhf RFID in practice*. Newnes, 2012.
- [10] Weixiu Du and Rodney Lynn Kirlin. Improved spatial smoothing techniques for doa estimation of coherent signals. *IEEE Transactions on signal processing*, 39(5):1208–1210, 1991.
- [11] Klaus Finkenzeller. *RFID handbook: fundamentals and applications in contactless smart cards, radio frequency identification and near-field communication.* John wiley & sons, 2010.
- [12] Gary M Gaukler and Ralf W Seifert. Applications of rfid in supply chains. *Trends in supply chain design and management*, pages 29–48, 2007.

- [13] R Ghayoula, N Fadlallah, A Gharsallah, and M Rammal. Phase-only adaptive nulling with neural networks for antenna array synthesis. *IET microwaves, antennas & propagation*, 3(1):154–163, 2009.
- [14] Gotmic AB. gssd0011. https://gotmic.se/ switches.html.
- [15] Randy L Haupt. Phase-only adaptive nulling with a genetic algorithm. *IEEE Transactions on Antennas and Propagation*, 45(6):1009–1015, 1997.
- [16] Elisabeth Ilie-Zudor, Zsolt Kemény, Fred Van Blommestein, László Monostori, and André Van Der Meulen. A survey of applications and requirements of unique identification systems and rfid techniques. *Computers in Industry*, 62(3):227–252, 2011.
- [17] Bryce Kellogg, Aaron Parks, Shyamnath Gollakota, Joshua R Smith, and David Wetherall. Wi-fi backscatter: Internet connectivity for rf-powered devices. In *Proceedings of the 2014 ACM Conference on SIGCOMM*, pages 607–618, 2014.
- [18] Bryce Kellogg, Vamsi Talla, Shyamnath Gollakota, and Joshua R Smith. Passive {Wi-Fi}: Bringing low power to {Wi-Fi} transmissions. In 13th USENIX Symposium on Networked Systems Design and Implementation (NSDI 16), pages 151–164, 2016.
- [19] Ghenadii Korotcenkov. *Handbook of humidity measurement, volume 2: Electronic and electrical humidity sensors.* CRC Press, 2019.
- [20] Manikanta Kotaru, Kiran Joshi, Dinesh Bharadia, and Sachin Katti. Spotfi: Decimeter level localization using wifi. In Proceedings of the 2015 ACM Conference on Special Interest Group on Data Communication, pages 269–282, 2015.
- [21] Han-il Lee, Tae-young Choi, Saeed Mohammadi, and Linda PB Katehi. An extremely low power 2 ghz cmos lc vco for wireless communication applications. In *The European Conference on Wireless Technology*, 2005., pages 31–34. IEEE, 2005.
- [22] Bo Li, Tara N Sainath, Ron J Weiss, Kevin W Wilson, and Michiel Bacchiani. Neural network adaptive beamforming for robust multichannel speech recognition. 2016.
- [23] Zhengxiong Li, Baicheng Chen, Zhuolin Yang, Huining Li, Chenhan Xu, Xingyu Chen, Kun Wang, and Wenyao Xu. Ferrotag: A paper-based mmwave-scannable tagging infrastructure. In *Proceedings of the 17th Confer*ence on Embedded Networked Sensor Systems, pages 324–337, 2019.

- [24] Libero. Soc v11.8 archive. https://www. microsemi.com/product-directory/root/ 5485-libero-soc-v11-8-archive.
- [25] Vincent Liu, Aaron Parks, Vamsi Talla, Shyamnath Gollakota, David Wetherall, and Joshua R Smith. Ambient backscatter: Wireless communication out of thin air. ACM SIGCOMM computer communication review, 43(4):39-50, 2013.
- [26] Sohrab Madani, Suraj Jog, Jesus O Lacruz, Joerg Widmer, and Haitham Hassanieh. Practical null steering in millimeter wave networks. In 18th USENIX Symposium on Networked Systems Design and Implementation (NSDI 21), pages 903–921, 2021.
- [27] Mohammad H. Mazaheri, Soroush Ameli, Ali Abedi, and Omid Abari. A millimeter wave network for billions of things. SIGCOMM '19, 2019.
- [28] Mohammad Hossein Mazaheri, Alex Chen, and Omid Abari. mmtag: a millimeter wave backscatter network. In Proceedings of the 2021 ACM SIGCOMM 2021 Conference, pages 463-474, 2021.
- [29] Moctar Mouhamadou, Patrick Vaudon, and Mohammed Rammal. Smart antenna array patterns synthesis: Null steering and multi-user beamforming by phase control. Progress In Electromagnetics Research, 60:95-106, 2006.
- [30] Pavel V Nikitin and KV Seshagiri Rao. Theory and measurement of backscattering from rfid tags. IEEE Antennas and Propagation Magazine, 48(6):212-218, 2006.
- [31] Thomas Nitsche, Guillermo Bielsa, Irene Tejado, Adrian Loch, and Joerg Widmer. Boon and bane of 60 ghz networks: Practical insights into beamforming, interference, and frame level operation. In Proceedings of the 11th ACM Conference on Emerging Networking Experiments and Technologies, CoNEXT '15, New York, NY, USA, 2015. Association for Computing Machinery.
- [32] Thomas Nitsche, Carlos Cordeiro, Adriana B Flores, Edward W Knightly, Eldad Perahia, and Joerg C Widmer. Ieee 802.11 ad: directional 60 ghz communication for multi-gigabit-per-second wi-fi. IEEE Communications Magazine, 52(12):132-141, 2014.
- [33] Joseph A Paradiso and Thad Starner. Energy scavenging for mobile and wireless electronics. IEEE Pervasive computing, 4(1):18–27, 2005.
- [34] Ioannis Pefkianakis and Kyu-Han Kim. Accurate 3d localization for 60 ghz networks. In Proceedings of the 16th ACM Conference on Embedded Networked Sensor Systems, pages 120-131, 2018.

- [35] Eldad Perahia, Carlos Cordeiro, Minyoung Park, and L Lily Yang. Ieee 802.11 ad: Defining the next generation multi-gbps wi-fi. In 2010 7th IEEE consumer communications and networking conference, pages 1–5. IEEE, 2010.
- [36] S. K. Saha, H. Assasa, A. Loch, N. M. Prakash, R. Shyamsunder, S. Aggarwal, D. Steinmetzer, D. Koutsonikolas, J. Widmer, and M. Hollick. Fast and infuriating: Performance and pitfalls of 60 ghz wlans based on consumer-grade hardware. In 2018 15th Annual IEEE International Conference on Sensing, Communication, and Networking (SECON), pages 1–9, 2018.
- [37] S. K. Saha, V. V. Vira, A. Garg, and D. Koutsonikolas. A feasibility study of 60 ghz indoor wlans. In 2016 25th International Conference on Computer Communication and Networks (ICCCN), pages 1–9, Aug 2016.
- [38] Swetank Kumar Saha, Yasaman Ghasempour, Muhammad Kumail Haider, Tariq Siddiqui, Paulo De Melo, Neerad Somanchi, Luke Zakrajsek, Arjun Singh, Owen Torres, Daniel Uvaydov, Josep Miquel Jornet, Edward Knightly, Dimitrios Koutsonikolas, Dimitris Pados, and Zhi Sun. X60: A programmable testbed for wideband 60 ghz wlans with phased arrays. In *Proceedings of the* 11th Workshop on Wireless Network Testbeds, Experimental Evaluation and CHaracterization, WiNTECH '17, page 75–82, New York, NY, USA, 2017. Association for Computing Machinery.
- [39] Swetank Kumar Saha, Tariq Siddiqui, Dimitrios Koutsonikolas, Adrian Loch, Joerg Widmer, and Ramalingam Sridhar. A detailed look into power consumption of commodity 60 ghz devices. In 2017 IEEE 18th International Symposium on A World of Wireless, Mobile and Multimedia Networks (WoWMoM), pages 1–10. IEEE, 2017.
- [40] Tie-Jun Shan and Thomas Kailath. Adaptive beamforming for coherent signals and interference. IEEE Transactions on Acoustics, Speech, and Signal Processing, 33(3):527–536, 1985.
- [41] Elahe Soltanaghaei, Akarsh Prabhakara, Artur Balanuta, Matthew Anderson, Jan M Rabaey, Swarun Kumar, and Anthony Rowe. Millimetro: mmwave retro-reflective tags for accurate, long range localization. In Proceedings of the 27th Annual International Conference on Mobile Computing and Networking, pages 69–82, 2021.
- [42] Daniel Steinmetzer, Daniel Wegemer, Matthias Schulz, Joerg Widmer, and Matthias Hollick. Compressive millimeter-wave sector selection in off-the-shelf ieee 802.11ad devices. In Proceedings of the 13th International Conference on Emerging Networking EXperiments and Technologies, CoNEXT '17, page 414-425,

- New York, NY, USA, 2017. Association for Computing Machinery.
- [43] Sanjib Sur, Ioannis Pefkianakis, Xinyu Zhang, and Kyu-Han Kim. Towards scalable and ubiquitous millimeterwave wireless networks. In *Proceedings of the 24th Annual International Conference on Mobile Computing and Networking*, pages 257–271, 2018.
- [44] Sanjib Sur, Vignesh Venkateswaran, Xinyu Zhang, and Parmesh Ramanathan. 60 ghz indoor networking through flexible beams: A link-level profiling. In *Proceedings of the 2015 ACM SIGMETRICS International Conference on Measurement and Modeling of Computer Systems*, SIGMETRICS '15, page 71–84, New York, NY, USA, 2015. Association for Computing Machinery.
- [45] Sanjib Sur, Xinyu Zhang, Parmesh Ramanathan, and Ranveer Chandra. Beamspy: enabling robust 60 ghz links under blockage. In *13th USENIX Symposium on Networked Systems Design and Implementation (NSDI 16)*, pages 193–206. USENIX Association, 2016.
- [46] Vamsi Talla, Mehrdad Hessar, Bryce Kellogg, Ali Najafi, Joshua R Smith, and Shyamnath Gollakota. Lora backscatter: Enabling the vision of ubiquitous connectivity. Proceedings of the ACM on interactive, mobile, wearable and ubiquitous technologies, 1(3):1–24, 2017.
- [47] Tong Van Luyen and Truong Vu Bang Giang. Interference suppression of ula antennas by phase-only control using bat algorithm. *IEEE Antennas and Wireless Propagation Letters*, 16:3038–3042, 2017.
- [48] Jie Xiong and Kyle Jamieson. {ArrayTrack}: A {Fine-Grained} indoor location system. In *10th USENIX Symposium on Networked Systems Design and Implementation (NSDI 13)*, pages 71–84, 2013.
- [49] Hao Xu, Vikas Kukshya, and Theodore S Rappaport. Spatial and temporal characteristics of 60-ghz indoor channels. *IEEE Journal on selected areas in communications*, 20(3):620–630, 2002.
- [50] Y Xu and Q Zhaojun. Research on interference test of 24ghz millimeter wave radar to 5g equipment. In Journal of Physics: Conference Series, volume 1584, page 012028. IOP Publishing, 2020.
- [51] Shiwen Yang, Yeow Beng Gan, and Anyong Qing. Antenna-array pattern nulling using a differential evolution algorithm. *International Journal of RF and Microwave Computer-Aided Engineering: Co-sponsored by the Center for Advanced Manufacturing and Packaging of Microwave, Optical, and Digital Electronics (CAMPmode) at the University of Colorado at Boulder,* 14(1):57–63, 2004.

- [52] D. Zhang, P. S. Santhalingam, P. Pathak, and Z. Zheng. Characterizing interference mitigation techniques in dense 60 ghz mmwave wlans. In 2019 28th International Conference on Computer Communication and Networks (ICCCN), pages 1–9, 2019.
- [53] Pengyu Zhang, Dinesh Bharadia, Kiran Joshi, and Sachin Katti. Hitchhike: Practical backscatter using commodity wifi. SenSys '16, 2016.
- [54] Pengyu Zhang, Colleen Josephson, Dinesh Bharadia, and Sachin Katti. Freerider: Backscatter communication using commodity radios. In *Proceedings of the* 13th International Conference on emerging Networking EXperiments and Technologies, pages 389–401, 2017.
- [55] Jia Zhao, Wei Gong, and Jiangchuan Liu. Spatial stream backscatter using commodity wifi. In Proceedings of the 16th Annual International Conference on Mobile Systems, Applications, and Services, pages 191–203, 2018.
- [56] Jia Zhao, Wei Gong, and Jiangchuan Liu. X-tandem: Towards multi-hop backscatter communication with commodity wifi. In *Proceedings of the 24th Annual Interna*tional Conference on Mobile Computing and Networking, pages 497–511, 2018.
- [57] Renjie Zhao, Timothy Woodford, Teng Wei, Kun Qian, and Xinyu Zhang. M-cube: A millimeter-wave massive mimo software radio. In *Proceedings of the 26th Annual International Conference on Mobile Computing and Networking*, MobiCom '20, New York, NY, USA, 2020. Association for Computing Machinery.
- [58] Yibo Zhu, Zengbin Zhang, Zhinus Marzi, Chris Nelson, Upamanyu Madhow, Ben Y. Zhao, and Haitao Zheng. Demystifying 60ghz outdoor picocells. In *Proceedings of the 20th Annual International Conference on Mobile Computing and Networking*, MobiCom '14, page 5–16, New York, NY, USA, 2014. Association for Computing Machinery.

Appendix A1

Estimating the AoA of incoming signals. We adopt a power delay profile-based solution (used for beam alignment in [43] and localization in [34]) for the purpose. As shown in Fig. 26, each peak in power delay profile corresponds to a path taken by the transmitted signal and arriving at different times at the receiver. The amplitude of each peak depends on

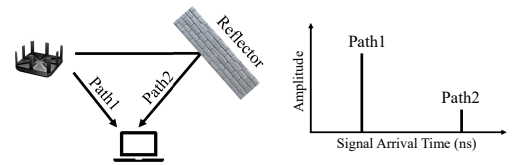


Figure 26: A power delay profile of incoming signals. the gain of the antenna beam pattern toward the path direction.

Even for different beam patterns, the relative time difference between the peaks remains unchanged and only the amplitude is affected. With K paths and different time delay Δt_d for each path and angle of arrival θ_i , the received signal with the m^{th} beam pattern can be expressed as:

$$y(t) = \sum_{i=1}^{K} \sum_{\mathbf{\theta}} A_m(\theta_i^{az}, \theta_i^{el}) \cdot h_i(\theta_i^{az}, \theta_i^{el}) \cdot x(t - \Delta t_{d_i})$$
(4)

where $A_m(\theta_i^{az}, \theta_i^{el})$ and $h_i(\theta_i^{az}, \theta_i^{el})$ is the gain of m^{th} beam and the complex channel gain, respectively. If we measure the power delay profile with different receive beams m=1,...,M, each measurement provides a set of peaks $Amp_m=\{a_{m,1},a_{m,2},...,a_{m,k}\}$. Hence, we can collect the amplitude set $Amp_{m,k}=\{a_{1,k},a_{2,k},...,a_{M,k}\}$ with M beam patterns for k^{th} path. Due to the different gain of m^{th} beam for different AoA, the peaks will have different amplitudes for the same physical paths. Hence, we can utilize this to estimate the AoA by comparing the normalized amplitude set $Amp'_{m,k}=\frac{Amp_{m,k}}{min(Amp_{m,k})}$ and beam pattern gain $G'_{m,\theta}=\frac{G_{m,\theta}}{min(G_{m,\theta})}$ where $G_{m,\theta}$ denotes the gain of m^{th} beam pattern toward θ . Hence, the angle of arrival θ_k of k^{th} path can be determined by solving following optimization:

$$\theta_k = \arg\min_{\theta} |Amp'_{m,k} - G'_{m,\theta}|^2 \tag{5}$$

Equ. 5 searches for a discrete angle θ_k that provides a minimum error between the measured CIR and beam pattern. Given this is a non-linear error curve fitting problem, we use the least mean square algorithm to find an approximate solution.

Appendix A2

Different Rx devices. As discussed in Sec. 5, we use two types of Rx devices: commodity 802.11ad AP from Airfide and the one with SiversIMA RF frontend. Since both have different types of antenna arrays, we compare their performance in terms of SINR when nulling is performed. We create custom beam patterns based on different tag positions (different backscatter and self-interference angles). For a fair comparison, we use 2-bit phase resolution (maximum for Airfide) on both. Fig. 27 shows a comparison of the two devices for an example beam pattern as well as SINR for three cases: (i) beam without nulling, (ii) custom beam on Airfide with nulling, and (iii) custom beam on SiversIMA with nulling. We find that our nulling and backscatter beamforming improves the SINR on both Rx devices. SiversIMA achieves a higher SINR due to the greater number of elements compared to Airfide.

Number and size of subarrays in spatial smoothing. Figure 28(a) illustrates the impact of different numbers and sizes of subarrays used for spatial smoothing in decorrelating incoming signals. We use the SiversIMA RF frontend with 16 antenna elements and form different combinations of subarrays. Initially, we evaluate the performance without spatial smoothing, i.e., using correlated signals for beam creation. We find that the average SINR nulling performance for a given

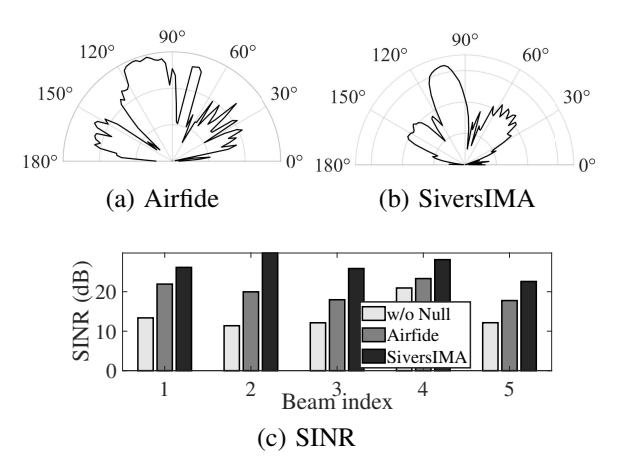


Figure 27: Backscatter SINR for different Rx devices.

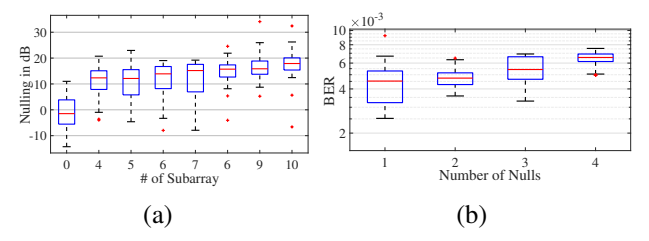


Figure 28: Nulling performance and backscatter BER for different (a) number of subarrays and (b) number of nulls.

tag direction and self-interference is -1.4 dB. Next, we create different numbers and sizes of subarrays where the size of each subarray is determined as L-N+1, where L and N are the total numbers of antenna elements and the number of subarrays, respectively. For instance, four subarrays imply that the size of each subarray is 13 elements. As demonstrated in Figure 28(a), average nulling performance improves by 6.5 dB as the number of subarrays increases from 4 to 10. Theoretically, n antenna elements provide a gain of 10, log, n dB. Therefore, the gain reduction from using 7 elements instead of 16 elements is 3.5 dB. However, spatial smoothing enhances the nulling performance by 18.5 dB due to better beam design after decorrelating the signals.

Multiple self-interference paths. In indoor scenarios, there can be multiple paths between a Tx and Rx position, even though not all paths are active simultaneously due to the directionality of Tx and Rx. To handle this, mmComb needs to generate Rx beams that can create nulls in multiple directions while still maintaining high gain towards the tag. To evaluate this, we set up an indoor environment where the tag's direction can be one of nine possible angles (depending on tag position), while the self-interference comes from 1, 2, 3, or 4 paths simultaneously out of 8 possible angles. Based on the number and angle of paths, we calculate the Rx beam pattern with multiple nulls. Fig. 28(b) shows the backscatter BER for different numbers of nulls. As expected, the BER increases as the number of nulls increases, but even with four nulls, the average BER remains 6.5×10^{-3} . This indicates that mmComb

can improve the SINR by suppressing self-interference, even in situations with severe multipath propagation.

Appendix A3

Impact on existing mmWave WiFi. As mmComb is designed to integrate tags into existing mmWave WiFi networks by reusing existing signals, we need to evaluate the potential impact of a tag's operation on other devices in the network. Since the tag responds to beamforming frames from the AP, a potential issue could arise where the tag's operations affect the beamforming between the AP and a client device (a receiver not intended to receive from the tag). As shown in Fig. 1 earlier, such a client device operates in quasi-omni mode when the AP sends out the beamforming frames, making it more susceptible to receiving backscatter data from surrounding tags.

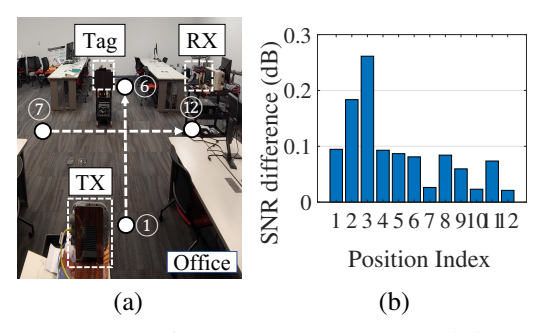


Figure 29: Impact of mmComb on mmWave WiFi: (a) experiment setting and (b) SNR different in beamforming

To evaluate the impact of tag operation on other devices in the mmWave WiFi network, we created a scenario where the AP and a client (not a tag receiver) were interested in performing beamforming, and the tag's operation could result in incorrect SNR measurements at the client. The client uses quasi-omni patterns and faces the tag to evaluate the worst-case impact of the tag operation. As shown in Fig. 29(a), the

AP (Tx) is located close to position 1. The tag is located at a 2.5m distance from the Tx. The Rx is moved from positions 1 through 12.

Fig. 29(b) shows the difference in SNR observed by the Rx from the AP with and without tag operation. We find that the SNR difference introduced by the tag operation is on average 0.18 dB for locations 1-3 and 0.06 dB for locations 4-10. The mean difference is no more than 0.19 dB. Therefore, we concluded that the tag operations do not negatively impact the beamforming between WLAN devices because when the client operates in the quasi-omni beam, the backscattered signal from the tag to the client is much weaker compared to the direct signal from the AP. Consequently, tags can coexist in a mmWave WiFi network without causing significant interference.

Appendix A4

Fig. 30 shows examples of six beam patterns before and after nulling with 4-bit phase resolution. The tag directions are $\{-45^{\circ}, -30^{\circ}, -15^{\circ}, 0^{\circ}, 15^{\circ}, 45^{\circ}\}$ for each patterns, while having a self-interference direction at $\{-15^{\circ}, 30^{\circ}, 15^{\circ}, 15^{\circ}, 60^{\circ}, 20^{\circ}\}$ accordingly.

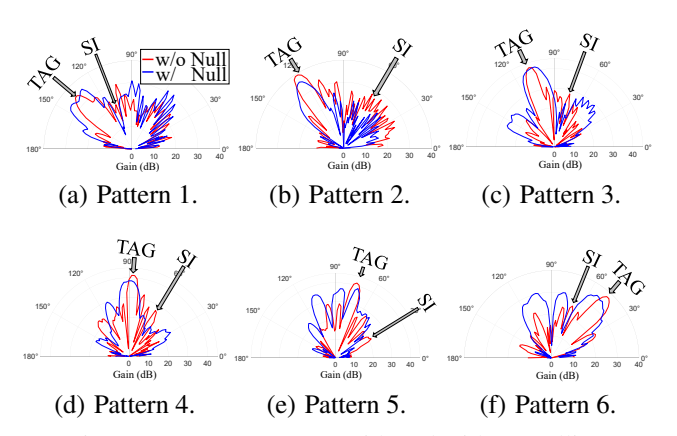


Figure 30: Beam patterns with and without nulling.